Efficient multi-domain bivariate spectral collocation solution for MHD laminar natural convection flow from a vertical permeable flat plate with uniform surface temperature and thermal radiation

S. Mondal[1], S.P. Goqo†* [1], P. Sibanda[1] and S.S. Motsa[1]

[1]School of Mathematics, Statistics and Computer Sciences, University of KwaZulu-Natal, Private Bag X01, Scottsville 3209, Pietermaritzburg, South Africa
[1]*Presenting author: spgoqo@gmail.com
[1]†Corresponding author: spgoqo@gmail.com

Abstract

A recently developed numerical method, multidomain quasilinearisation method, is applied on a steady laminar, natural convection boundary layer flow of MHD viscous and incompressible fluid from a vertical permeable flat plate with uniform temperature in this paper. Non-dimensionless variables are used to transform the governing equations to a system of non-dimensional nonlinear partial differential equations. Then the resulting equations are solved numerically by using multidomain quasilinearisation method. The numerical results for tangential velocity, transverse velocity, and temperature, skin friction and Nusselt number are calculated and shown in a table and in various graphs.

Keywords: Natural convection; Magnetohydrodynamics; Multi-domain; Thermal radiation; Boundary layer.

Nomenclature

B	Magnetic induction
C_{fx}	Local skin friction
e	Electronic charge
E	Intensity of electric field
g	Gravitational acceleration
Gr_x	Modified Grashof number
H	Magnetic intensity
J	Electric current density
m	Hall parameter
M	Magnetic parameter
Nu_x	Local Nusselt number
p	Pressure
P_r	Prandtl number
T	Temperature of the fluid
$T\infty$	Free stream temperature
x, y, z	Co-ordinate directions
u, v, w	Velocity components in x, y, z directions
v	Velocity component normal to u
V	Transpiration velocity
x	Axial coordinate
y	Coordinate normal to x
q_r	Thermal radiation
R	Thermal radiation parameter

Greek symbols

α	Thermal diffusivity
β	Volumetric expansion coefficient for temperature
ψ	Stream function
θ	Dimensionless temperature function
ρ	Density
ν	Kinematic viscosity
μ	Dynamic viscosity
ξ	Transpiration parameter
η	Pseudo similarity variable

Subscripts

w	Conditions at wall
∞	Conditions far away from wall

Introduction

In many industrial processes, the study of magnetohydrodynamics natural convection flow and heat transfer has attracted considerable attention during the last decades. This is due to its applications which are found in MHD generator, flight MHD, Plasma studies, nuclear reactors, geothermal extractions, Hall accelerators and boundary layer control in the field of aeronautics and aerodynamics. Another important application of magnetohydrodynamic natural convection boundary layer flow past a semi-infinite vertical permeable flat plate with uniform mass flux is in space flight and in nuclear reactor. This applications normally requires a strong magnetic field and a low density gas and therefore the Hall current and ion slip becomes important.

The natural convection boundary layer flow from a vertical wall with Hall current and heat flux has been discussed by Sato [1], Yamanishi [2], Sherman and Sutton [3], Sing and Cowling [4], Sparrow and Cess [5], Gupta [6]. Free convection flow of a conducting fluid permeated by a transverse magnetic field was studied by Katagiri [7]. It has been observed by Singh and Cowling [4] that regardless of the strength of the applied magnetic field there will always be a region in the neighborhood of the leading edge of the plate where electromagnetic force are unimportant, whilst at large distances from the leading edge this magnetic force dominate. Pop and Watanabe analyzed the free convection flow of a conducting fluid permeated by a transverse magnetic field in the presence of Hall effects and uniform magnetic field.

Numerical solutions of MHD convection and mass transfer flow of viscous incompressible fluid were studied by Wahiduzzaman et al. [9]. They assumed that the induced magnetic field is negligible compared with the imposed magnetic field. Saha et al also studied the effect of Hall current on the steady, laminar, natural convection boundary layer flow of MHD viscous and incompressible fluid from a semi-infinite heated permeable vertical flat plate with an applied magnetic field transverse to it has been investigated, assuming that the induced magnetic field is negligible compared to the imposed magnetic field.

In the design of nuclear plants, gas turbines, propulsion devises for aircraft, missiles, satellites, and space vehicles, radiative heat transfer is a very important factor. This is due to the non-isothermal effects where high temperature is involved. Most studies that involve thermal radiation have been mostly limited to a stretching sheet. Some of the important investigations involving thermal radiation effects can be found in, for example, Englang and Emery [10], Gorla and Pop [11], Raptis [12], Abd El-Aziz [13, 14, 15].

Most of these studies rely on traditional numerical methods which requires the use of many grid points for accurate solutions. This is the result of the presence of local variable ξ which does not give accurate results for, usually, values of $\xi > 1$ [17]. The present study attempts to obtain the accurate solution with the use of few grid points.

It has been demonstrated that the finite difference method gives the solutions for all large values of transpiration parameter ξ. However, nonsimilarity method cannot give solutions for large values of ξ [16]. The aim of this paper is to give an alternative method that will handle solutions for large values of ξ when nonsimilarity transformation methods are used.

Problem Formulation

Consider the steady natural convection boundary layer flow of an electrically conducting and viscous incompressible fluid from a semi-infinite heated permeable vertical flat plate in presence of magnetic field and thermal radiation with the effect of Hall currents.

Applying the Boussinesq approximation, the boundary layer equations governing the flow under the assumption that the fluid is quasi-neutral and ion slip and thermoelectric effect results in the following system of equations:

$$\frac{\partial u}{\partial x} + \frac{\partial v}{\partial y} = 0, \tag{1}$$

$$u\frac{\partial u}{\partial x} + v\frac{\partial u}{\partial y} = \nu\frac{\partial^2 u}{\partial y^2} + g\beta(T - T_\infty) - \frac{\sigma B_0^2}{\rho(1+m^2)}(u + mw), \tag{2}$$

$$u\frac{\partial w}{\partial x} + v\frac{\partial w}{\partial y} = \nu\frac{\partial^2 w}{\partial y^2} + \frac{\sigma B_0^2}{\rho(1+m^2)}(mu - w), \tag{3}$$

$$u\frac{\partial T}{\partial x} + v\frac{\partial T}{\partial y} = \alpha\frac{\partial^2 T}{\partial y^2} - \frac{1}{\rho c_p}\frac{\partial q_r}{\partial y}, \tag{4}$$

$$\tag{5}$$

where u, v and w are the velocities in the $x-$,$y-$ and $z-$ direction, T is the fluid temperature, $\nu(= \mu/\rho)$ is the kinematic coefficient of viscosity, μ is the fluid viscocity and ρ is the fluid density, $\alpha(= \kappa/\rho c_p)$ is the thermal diffusivity with κ being the fluid thermal conductivity and c_p is the heat capacity of the fluid at constant pressure, q_r is the thermal radiative heat flux, $m(= \omega^2\tau^2)$ is the Hall parameter, with ω as the cyclotron frequency of electron and τ as collision time of electrons with ions.

The radiative heat flux q_r under Rosseland approximation takes the form

$$q_r = -\frac{4\sigma}{3k_1}\frac{\partial T^4}{\partial y}, \tag{6}$$

where σ is the Stefan-Boltzmann constant and k_1 is the mean absorption coefficient. Assuming that the temperature difference within the flow is sufficiently small, T^4 may be approximated in Taylor series form, after ignoring higher order terms, as follows:

$$T^4 = 4T_\infty^3 T - 3T_\infty^4. \tag{7}$$

Applying (6) and (7) to equation (4) we get

$$u\frac{\partial T}{\partial x} + v\frac{\partial T}{\partial y} = \alpha\frac{\partial^2 T}{\partial y^2} - \frac{16\sigma T_\infty^3}{3k_1\rho c_p}\frac{\partial^2 T}{\partial y^2}. \tag{8}$$

The boundary conditions are:

$$u(x,y)=0,\ \ v(x,y)=-V_0,\ \ w(x,y)=0,\ \ T(x,y)=T_w\ \text{ at } y=0 \tag{9}$$
$$u(x,y)=0,\ \ v(x,y)=0,\ \ w(x,y)=0,\ \ T(x,y)=T_\infty\ \text{ at } y=\infty, \tag{10}$$

where V_0 is the transpiration velocity which is positive for suction and negative for injection.

The set of non-linear partial differential equations are transformed by introduction of dimensionless group of transformations for the dependent and independent variables applicable in natural convection flow from a vertical surface:

$$\psi(x,y)=\nu Gr_x^{1/4}[f(\xi,\eta)+\xi],\ \ \eta=\frac{y}{x}Gr_x^{1/4},\ \ \xi=\frac{V_0 x}{\nu}Gr_x^{-1/4}, \tag{11}$$
$$w(x,y)=\frac{\nu}{x}Gr_x^{1/2}g(\xi,\eta), \theta=\frac{T-T_\infty}{T_w-T_\infty} \tag{12}$$

where ψ is the stream function, defined by

$$u=\frac{\partial\psi}{\partial y}\ \text{ and }\ v=-\frac{\partial\psi}{\partial x} \tag{13}$$

which satisfies the continuity condition (1). In the above equation (12) f is the dimensionless stream function, g is the dimensionless velocity and θ is the dimensionless temperature of the fluid. η is the pseudo-similarity variable and ξ is the transpiration parameter depending on the transpiration velocity V_0 and the axial variable x.

Applying these transformations to the system of equations (2) - (4), the resulting governing non-similarity system of partial differential equations are expressed in dimensionless form as [17]:

$$f'''+\frac{3}{4}ff''-\frac{1}{2}f'^2+\theta+\xi f''-\frac{M}{(1-m^2)}(f'+mg)=\frac{1}{4}\xi\left(f'\frac{\partial f'}{\partial\xi}-f''\frac{\partial f}{\partial\xi}\right), \tag{14}$$
$$g''+\frac{3}{4}fg'-\frac{1}{2}f'g+\xi g'-\frac{M}{(1-m^2)}(g-mf')=\frac{1}{4}\xi\left(f'\frac{\partial g}{\partial\xi}-g'\frac{\partial f}{\partial\xi}\right) \tag{15}$$
$$\frac{1}{Pr}\left(1+\frac{3}{4}R\right)\theta''+\frac{3}{4}f\theta'+\xi\theta'=\frac{1}{4}\xi\left(f'\frac{\partial\theta}{\partial\xi}-\theta'\frac{\partial f}{\partial\xi}\right) \tag{16}$$

where the local Grashof number, magnetic field number and thermal radiation parameter are, respectively, given by

$$Gr_x=\frac{g\beta\delta T}{\nu^2}x^3,\qquad M=\frac{\sigma B_0^2x^2}{\rho Gr_x^{\frac{1}{2}}},\qquad R=\frac{4\sigma T_\infty^3}{kk_1} \tag{17}$$

The primes in the above equations denoted differentiation with respect to η and the correspond-

ing boundary conditions are given by

$$f(0,\xi) = f'(0,\eta) = 0, \quad g(0,\xi) = \theta(0,\xi) = 1, \tag{18}$$

$$f'(\infty,\xi) = g(\infty,\xi) = \theta(\infty,\xi) = 0. \tag{19}$$

The physical quantities of interest in this case are the skin-friction, Nusselt and Sherwood numbers which are defined in [23] as

$$C_{fx}Gr_x^{-3/4} = f''(0,\xi), \quad Nu_xGr_x^{-1/4} = -\theta'(0,\xi), \tag{20}$$

respectively.

Bivariate Spectral Quasilinearisation Method (BSQLM)

In this section we first describe the standard bivariate spectral quasilinearisation method for solving coupled non-linear partial differential equations. The quasi-linearisation method is based on Taylor series expansion of system of equations about some previous approximation of the solution. The assumption used is that the difference between the current and previous solution is small. To illustrate the idea of the BSQLM we first write equations as

$$\Omega_k[H_1, H_2, H_3] = 0, \quad \text{for} \quad k = 1, 2, 3, \tag{21}$$

where H_1, H_2 and H_3 represents equations (14), (15) and (16) respectively. The quasilinearisation scheme applied in equations (14) - (16) results in

$$a_{0r}f'''_{r+1} + a_{1r}f''_{r+1} + a_{2r}f'_{r+1} + a_{3r}f_{r+1} + a_{4r}\frac{\partial f_{r+1}}{\partial \xi} + a_{5r}\frac{\partial f'_{r+1}}{\partial \xi} + a_{6r}g_{r+1} + a_{7r}\theta_{r+1} = R_{1r}, \tag{22}$$

$$b_{0r}f'_{r+1} + b_{1r}f_{r+1} + b_{2r}\frac{\partial f_{r+1}}{\partial \xi} + b_{3r}g''_{r+1} + b_{4r}g'_{r+1} + b_{5r}g_{r+1} + b_{6r}\frac{\partial g_{r+1}}{\partial \xi} + b_{7r}\theta_{r+1} = R_{2r}, \tag{23}$$

$$c_{0r}f'_{r+1} + c_{1r}f_{r+1} + c_{2r}\frac{\partial f_{r+1}}{\partial \xi} + c_{3r}g_{r+1} + c_{4r}\theta''_{r+1} + c_{5r}\theta'_{r+1} + c_{6r}\theta_{r+1} + c_{7r}\frac{\partial \theta_{r+1}}{\partial \xi} = R_{3r}, \tag{24}$$

where

$$a_{0r}=1,\;\; a_{1r}=\frac{3}{4}f_r+\xi+\frac{1}{4}\xi\frac{\partial f_r}{\partial \xi},\;\; a_{2r}=-f_r'-\frac{M}{1-m^2}-\frac{1}{4}\xi\frac{\partial f_r'}{\partial \xi},$$
$$a_{3r}=\frac{3}{4}f_r'',\;\; a_{4r}=\frac{1}{4}\xi f_r'',\;\; a_{5r}=-\frac{1}{4}\xi f_r'',\;\; a_{6r}=-\frac{Mm}{1+m^2},\;\; a_{7r}=1,$$
$$b_{0r}=-\frac{1}{2}g_r+\frac{Mm}{1+m^2}-\frac{1}{4}\xi\frac{\partial g_r}{\partial \xi},\;\; b_{1r}=\frac{3}{4}g_r',\;\; b_{2r}=\frac{1}{4}\xi g_r',$$
$$b_{3r}=1,\;\; b_{4r}=\frac{3}{4}f_r+\xi+\frac{1}{4}\xi\frac{\partial f_r}{\partial \xi},\;\; b_{5r}=-\frac{1}{2}f_r'-\frac{M}{1+m^2},\;\; b_{6r}=-\frac{1}{4}\xi f_r',\;\; b_{7r}=0,$$
$$c_{0r}=-\frac{1}{4}\xi\frac{\partial \theta_r}{\partial \xi},\;\; c_{1r}=\frac{3}{4}\theta_r',\;\; c_{2r}=\frac{1}{4}\xi\theta_r',\;\; c_{3r}=0,$$
$$c_{4r}=\frac{1}{Pr}(1+\frac{4}{3}R),\;\; c_{5r}=\frac{3}{4}f_r+\xi+\frac{1}{4}\xi f_r'.$$
$$R_{1r}=a_{0r}f_r'''+a_{1r}f_r''+a_{2r}f_r'+a_{3r}f_r+a_{4r}\frac{\partial f_r}{\partial \xi}+a_{5r}\frac{\partial f_r'}{\partial \xi}+a_{6r}g_{r+1}+a_{7r}\theta_{r+1}-H_1,$$
$$R_{2r}=b_{0r}f_r'+b_{1r}f_r+b_{2r}\frac{\partial f_r}{\partial \xi}+b_{3r}g_r''+b_{4r}g_r'+b_{5r}g_r+b_{6r}\frac{\partial g_r}{\partial \xi}+b_{7r}\theta_r-H_2,$$
$$R_{3r}=c_{0r}f_r'+c_{1r}f_r+c_{2r}\frac{\partial f_r}{\partial \xi}+c_{3r}g_r+c_{4r}\theta_r''+c_{5r}\theta_r'+c_{6r}\theta_r+c_{7r}\frac{\partial \theta_r}{\partial \xi}-H_3.$$

Applying spectral collocation on (14) - (16) gives

$$A_{11}\boldsymbol{F}_i+a_{4r}\sum_{j=0}^{Nt}d_{ij}\boldsymbol{F}_j+a_{5r}\sum_{j=0}^{Nt}d_{ij}\boldsymbol{D}\boldsymbol{F}_j+A_{12}\boldsymbol{G}_i+A_{13}\boldsymbol{\theta}_i=\boldsymbol{R}_{1,i},\tag{25}$$
$$A_{21}\boldsymbol{F}_i+b_{2r}\sum_{j=0}^{Nt}d_{ij}\boldsymbol{F}_j+A_{22}\boldsymbol{G}_i+b_{6r}\sum_{j=0}^{Nt}d_{ij}\boldsymbol{G}_j+A_{23}\boldsymbol{\theta}_i=\boldsymbol{R}_{2,i},\tag{26}$$
$$A_{31}\boldsymbol{F}_i+c_{2r}\sum_{j=0}^{Nt}d_{ij}\boldsymbol{F}_j+A_{32}\boldsymbol{G}_i+A_{33}\boldsymbol{\theta}_i+c_{7r}\sum_{j=0}^{Nt}d_{ij}\boldsymbol{\theta}_j=\boldsymbol{R}_{3,i},\tag{27}$$

where

$$A_{11}^i=\boldsymbol{a}_{0r}\boldsymbol{D}^3+\boldsymbol{a}_{1r}\boldsymbol{D}^2+\boldsymbol{a}_{2r}\boldsymbol{D}+\boldsymbol{a}_{3r}\boldsymbol{I},\;\; A_{12}^i=\boldsymbol{a}_{6r}\boldsymbol{I},\;\; A_{13}^i=\boldsymbol{a}_{7r}\boldsymbol{I},$$
$$A_{21}^i=\boldsymbol{b}_{0r}\boldsymbol{D}+\boldsymbol{b}_{1r}\boldsymbol{I},\;\; A_{22}=\boldsymbol{b}_{3r}\boldsymbol{D}^2+\boldsymbol{b}_{4r}\boldsymbol{D}+\boldsymbol{b}_{5r}\boldsymbol{I},\;\; A_{23}=\boldsymbol{b}_{7r}\boldsymbol{I},$$
$$A_{11}^i=\boldsymbol{c}_{0r}\boldsymbol{D}+\boldsymbol{c}_{1r}\boldsymbol{I},\;\; A_{32}=\boldsymbol{c}_{3r}\boldsymbol{I},\;\; A_{33}=\boldsymbol{c}_{4r}\boldsymbol{D}^2+\boldsymbol{c}_{5r}\boldsymbol{D}+\boldsymbol{c}_{6r}\boldsymbol{I}.$$

For convenience, equations (25), (26) and (27) are expanded for $i=0,\ldots,M_2$ and rearranged to obtain the following matrix form

$$\mathbf{B}_r\boldsymbol{X}_{r+1}=\mathbf{R}_r\tag{28}$$

where the coefficient matrix $\mathbf{B}_r$ is defined as

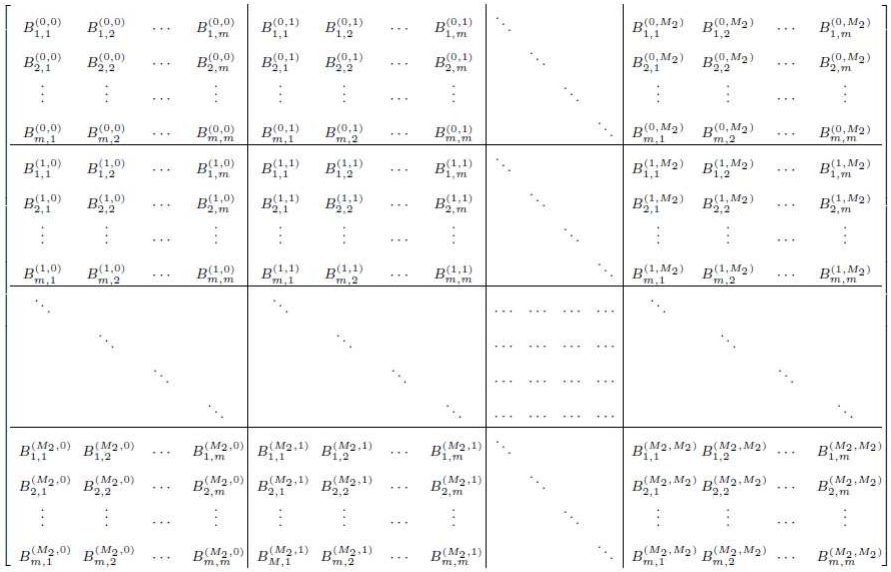

where

$$
\begin{aligned}
B_{11}^{ii} &= A_{11}^{i} + \boldsymbol{a}_{4r} d_{ii} \boldsymbol{I} + \boldsymbol{a}_{5r} d_{ii} \boldsymbol{D}, \quad B_{12}^{ii} = A_{12}^{i}, B_{13}^{ii} = A_{13}^{i}, \\
B_{11}^{ij} &= \boldsymbol{a}_{4r} d_{ij} \boldsymbol{I} + a_{5r} d_{ij} \boldsymbol{D}, \quad B_{12}^{ij} = 0, \quad B_{13}^{ij} = 0, \\
B_{21}^{ii} &= A_{21}^{i} + \boldsymbol{b}_{2r} d_{ii} \boldsymbol{I} \quad B_{22}^{ii} = A_{22}^{i} + \boldsymbol{b}_{6r} d_{ii} \boldsymbol{I}, B_{23}^{ii} = A_{23}^{i}, \\
B_{21}^{ij} &= \boldsymbol{b}_{2r} d_{ij} \boldsymbol{I}, \quad B_{22}^{ij} = \boldsymbol{6r} d_{ij} \boldsymbol{I}, \quad B_{23}^{ij} = 0, \\
B_{31}^{ii} &= A_{31}^{i} + \boldsymbol{c}_{2r} d_{ii} \boldsymbol{I}, \quad B_{32}^{ii} = A_{32}^{i}, B_{33}^{ii} = A_{33}^{i} + \boldsymbol{c}_{7r} d_{ii} \boldsymbol{I}, \\
B_{31}^{ij} &= \boldsymbol{c}_{2r} d_{ij} \boldsymbol{I}, \quad B_{32}^{ij} = 0, \quad B_{33}^{ij} = \boldsymbol{c}_{7r} d_{ij} \boldsymbol{I},
\end{aligned}
\tag{29}
$$

The vectors $\boldsymbol{X}_{r+1}$ and $\mathbf{R}_r$ are defined as

$$
\begin{aligned}
\boldsymbol{X}_{r+1} &= \left[\mathbf{F}_{1,r+1}^{(0)} \mathbf{G}_{2,r+1}^{(0)} \cdots \boldsymbol{\theta}_{m,r+1}^{(0)} \left| \mathbf{F}_{1,r+1}^{(1)} \mathbf{G}_{2,r+1}^{(1)} \cdots \boldsymbol{\theta}_{m,r+1}^{(1)} \right| \cdots\cdots\cdots\cdots \left| \mathbf{F}_{1,r+1}^{(M_2)} \mathbf{G}_{2,r+1}^{(M_2)} \cdots \boldsymbol{\theta}_{m,r+1}^{(M_2)} \right.\right]^T \\
\mathbf{R}_r &= \left[\mathbf{R}_1^{(0)} \ \mathbf{R}_2^{(0)} \ \mathbf{R}_3^{(0)} \cdots \mathbf{R}_m^{(0)} \left| \mathbf{R}_1^{(1)} \ \mathbf{R}_2^{(1)} \ \mathbf{R}_3^{(1)} \cdots \mathbf{R}_m^{(1)} \right| \cdots\cdots\cdots\cdots \left| \mathbf{R}_1^{(M_2)} \ \mathbf{R}_2^{(M_2)} \ \cdots \ \mathbf{R}_m^{(M_2)} \right.\right]^T
\end{aligned}
$$

The approximate solutions are obtained by solving (28) iteratively for $r = 0, 1, 2, \ldots$. The inclusion of boundary conditions and multi-domain solution approach is discussed in the next section through a specific example.

Multi-domain bivariate spectral collocation method for systems of PDEs

It is well-known that the standard form of the bivariate spectral quasi-linearisation method described in [24] works well for problem defined over small domains. Large domains require proportionally larger number of nodes to yield accurate results. For the BSQLM, increasing the number of nodes increases the computational effort required to solve the matrix equations almost exponentially. A simple way of ensuring that accurate solutions are obtained efficiently over large domains is to seek to limit the size of the matrix equations. As can be noted from matrix equation (28), the size of the coefficient matrix for a system of m PDEs in m unknowns is $m(M_1+1)(M_2+1)$ by $m(M_1+1)(M_2+1)$, where M_1, M_2 give the number of nodes in the x_1 and x_2 domains, respectively. Below, we introduce a strategy that seeks to reduce the size of the matrix equations by ensuring that the value of M_2 is kept to be as low as possible. For problems where the largest order of the derivative with respect to x_2 is one this can be achieved by evalu-

ating the solution in a sequence of equal intervals, which are subject to continuity conditions at the end points of each interval.

To apply the multi-domain bivariate spectral quasi-linearisation method (MD-BSQLM) we divide the interval $\xi \in [0, \xi_P]$ into P sub-intervals $\Omega_e = [\xi_{e-1}, \xi_e]$ for $e = 1, 2, \ldots, P$ as shown in the illustration 1 below.

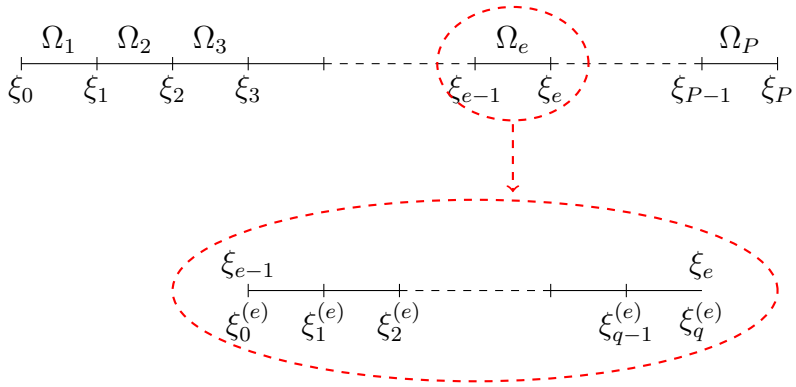

Figure 1: Multi-domain grid

Each interval Ω_e is further divided into q divisions which are not necessarily of equal spacing. The non-linear equations (25), (26) and (27) are solved in each subinterval $[\xi_{e-1}, \xi_e]$ with the solution denoted by $\overset{e}{f}(\eta, \xi)$ in this interval. In the first interval $[\xi_{e-1}, \xi_e]$, the solution is $\overset{1}{f}(\eta, \xi)$ is obtained subject to the "initial" condition $\overset{1}{f}(\eta, 0)$. For each $e \geq 2$, at each interval $[\xi_{e-1}, \xi_e]$, the continuity condition

$$\overset{e}{f}(\eta, \xi_{e-1}) = \overset{e-1}{f}(\eta, \xi_{e-1}) \tag{30}$$

is used to implement the BSQLM over the interval $[\xi_{e-1}, \xi_e]$. This process is repeated to generate a sequence of solutions $\overset{e}{f}(\eta, \xi)$ for $e = 1, 2, \ldots, P$

In our system, the number of equations and unknowns is $m = 3$ and the orders of the highest derivatives that are required as limits in the definition of the coefficient parameters and matrices are

$$n_{1,1} = 3, \quad n_{1,2} = 0, \quad n_{1,3} = 0, \quad n_{2,1} = 1, \quad n_{2,2} = 2 \quad n_{3,1} = 1, \quad n_{3,3} = 2$$

With these values, the coefficient parameters and matrices are obtained using the formulas given in the previous section and are defined in the appendix. Applying the spectral collocation gives

$$A_{11}\overset{e}{\boldsymbol{F}}_{i,r+1} + a_{4r}\sum_{j=0}^{M_2} d_{ij}\overset{e}{\boldsymbol{F}}_{j,r+1} + a_{5r}\sum_{j=0}^{M_2} d_{ij}\boldsymbol{D}\overset{e}{\boldsymbol{F}}_{j,r+1} + A_{12}\overset{e}{\boldsymbol{G}}_{i,r+1} + A_{13}\overset{e}{\boldsymbol{\theta}}_{i,r+1} = \overset{e}{\boldsymbol{R}}_{1,i}, \tag{31}$$

$$A_{21}\overset{e}{\boldsymbol{F}}_{i,r+1} + b_{2r}\sum_{j=0}^{M_2} d_{ij}\overset{e}{\boldsymbol{F}}_{j,r+1} + A_{22}\overset{e}{\boldsymbol{G}}_{i,r+1} + b_{6r}\sum_{j=0}^{M_2} d_{ij}\overset{e}{\boldsymbol{G}}_{j,r+1} + A_{23}\overset{e}{\boldsymbol{\theta}}_{i,r+1} = \overset{e}{\boldsymbol{R}}_{2,i}, \tag{32}$$

$$A_{31}\overset{e}{\boldsymbol{F}}_{i,r+1} + c_{2r}\sum_{j=0}^{M_2} d_{ij}\overset{e}{\boldsymbol{F}}_{j,r+1} + A_{32}\overset{e}{\boldsymbol{G}}_{i,r+1} + A_{33}\overset{e}{\boldsymbol{\theta}}_{i,r+1} + c_{7r}\sum_{j=0}^{M_2} d_{ij}\overset{e}{\boldsymbol{\theta}}_{j,r+1} = \overset{e}{\boldsymbol{R}}_{3,i}, \tag{33}$$

where

$$\mathbf{F}_{i,r+1} = [f_{r+1}(\hat{\xi}_i, \hat{\eta}_0), f_{r+1}(\hat{\xi}_i, \hat{\eta}_1), f_{r+1}(\hat{\xi}_i, \hat{\eta}_2), \ldots, f_{r+1}(\hat{\xi}_i, \hat{\eta}_{M_1})]^T,$$
$$\mathbf{G}_{i,r+1} = [g_{r+1}(\hat{\xi}_i, \hat{\eta}_0), g_{r+1}(\hat{\xi}_i, \hat{\eta}_1), g_{r+1}(\hat{\xi}_i, \hat{\eta}_2), \ldots, g_{r+1}(\hat{\xi}_i, \hat{\eta}_{M_1})]^T,$$
$$\boldsymbol{\theta}_{i,r+1} = [\theta_{r+1}(\hat{\xi}_i, \hat{\eta}_0), \theta_{r+1}(\hat{\xi}_i, \hat{\eta}_1), \theta_{r+1}(\hat{\xi}_i, \hat{\eta}_2), \ldots, \theta_{r+1}(\hat{\xi}_i, \hat{\eta}_{M_1})]^T.$$

The boundary conditions for solving equations (39) - (41) are

$$\overset{e}{f}(\xi_i, \eta_{M_1}) = 0, \qquad \sum_{p=0}^{M_1} \mathbf{D}^{(1,0)}_{M_1,p} \overset{e}{f}(\xi_i, \eta_p) = 0, \qquad \overset{e}{g}(\xi_i, \eta_{M_1}) = \overset{e}{\theta}(\xi_i, \eta_{M_1}) = 1, \tag{34}$$

$$\sum_{p=0}^{M_1} \mathbf{D}^{(1,0)}_{0,p} \overset{e}{f}(\xi_i, \eta_p) = 0, \qquad \overset{e}{g}(\xi_i, \eta_0) = \overset{e}{\theta}(\xi_i, \eta_0) = 0. \tag{35}$$

The "*initial*" conditions at $\xi = 0$ ($\hat{\xi} = \hat{\xi}_{M_2} = -1$) are obtained by solving the following ODE set

$$f''' + \frac{3}{4} f f'' - \frac{1}{2} f'^2 + \theta - \frac{M}{(1-m^2)}(f' + mg) = 0, \tag{36}$$
$$g'' + \frac{3}{4} f g' - \frac{1}{2} f' g - \frac{M}{(1-m^2)}(g - mf') = 0 \tag{37}$$
$$\frac{1}{Pr}\left(1 + \frac{3}{4}R\right)\theta'' + \frac{3}{4} f \theta' = 0 \tag{38}$$

The solution of equation (36) - (38), in the first interval, are denoted by $\overset{1}{\mathbf{F}}_{M_2,r+1}$, $\overset{1}{\boldsymbol{G}}_{M_2,r+1}$ and $\overset{1}{\boldsymbol{\theta}}_{M_2,r+1}$. In the next intervals we solve the following equations

$$A_{11}\overset{e}{\boldsymbol{F}}_{i,r+1} + a_{4r}\sum_{j=0}^{M_2-1} d_{ij}\overset{e}{\boldsymbol{F}}_{j,r+1} + a_{5r}\sum_{j=0}^{M_2-1} d_{ij}\boldsymbol{D}\overset{e}{\boldsymbol{F}}_{j,r+1} + A_{12}\overset{e}{\boldsymbol{G}}_{i,r+1} + A_{13}\overset{e}{\boldsymbol{\theta}}_{i,r+1} = \overset{e}{\boldsymbol{K}}_{1,i}, \tag{39}$$

$$A_{21}\overset{e}{\boldsymbol{F}}_{i,r+1} + b_{2r}\sum_{j=0}^{M_2-1} d_{ij}\overset{e}{\boldsymbol{F}}_{j,r+1} + A_{22}\overset{e}{\boldsymbol{G}}_{i,r+1} + b_{6r}\sum_{j=0}^{M_2-1} d_{ij}\overset{e}{\boldsymbol{G}}_{j,r+1} + A_{23}\overset{e}{\boldsymbol{\theta}}_{i,r+1} = \overset{e}{\boldsymbol{K}}_{2,i}, \tag{40}$$

$$A_{31}\overset{e}{\boldsymbol{F}}_{i,r+1} + c_{2r}\sum_{j=0}^{M_2-1} d_{ij}\overset{e}{\boldsymbol{F}}_{j,r+1} + A_{32}\overset{e}{\boldsymbol{G}}_{i,r+1} + A_{33}\overset{e}{\boldsymbol{\theta}}_{i,r+1} + c_{7r}\sum_{j=0}^{M_2-1} d_{ij}\overset{e}{\boldsymbol{\theta}}_{j,r+1} = \overset{e}{\boldsymbol{K}}_{3,i}, \tag{41}$$

where

$$\overset{e}{\mathbf{K}}_{1,i} = \overset{e}{\mathbf{R}}_{1,i} - a_{4r} d_{iM_2}\overset{e}{\boldsymbol{F}}_{M_2,r+1} - a_{5r} d_{iM_2}\boldsymbol{D}\overset{e}{\boldsymbol{F}}_{M_2,r+1}, \tag{42}$$
$$\overset{e}{\mathbf{K}}_{2,i} = \overset{e}{\mathbf{R}}_{2,i} - b_{2r} d_{iM_2}\overset{e}{\boldsymbol{F}}_{M_2,r+1} - b_{6r} d_{iM_2}\overset{e}{\boldsymbol{G}}_{M_2,r+1}, \tag{43}$$
$$\overset{e}{\mathbf{K}}_{3,i} = \overset{e}{\mathbf{R}}_{3,i} - c_{2r} d_{iM_2}\overset{e}{\boldsymbol{F}}_{M_2,r+1} - c_{7r} d_{iM_2}\overset{e}{\boldsymbol{\theta}}_{M_2,r+1}. \tag{44}$$

The continuity conditions in this example are given by

$$
\begin{aligned}
\overset{e}{f}(\eta, \xi_{e-1}) &= \overset{e-1}{f}(\eta, \xi_{e-1}), \\
\overset{e}{g}(\eta, \xi_{e-1}) &= \overset{e-1}{g}(\eta, \xi_{e-1}), \\
\overset{e}{\theta}(\eta, \xi_{e-1}) &= \overset{e-1}{\theta}(\eta, \xi_{e-1}),
\end{aligned} \tag{45}
$$

Applying the continuity conditions on (42) - (44) gives

$$
\overset{e}{\mathbf{K}}_{1,i} = \overset{e}{\mathbf{R}}_{1,i} - a_{4r} d_{iM_2} \overset{e-1}{\boldsymbol{F}}_{M_2,r+1} - a_{5r} d_{iM_2} \boldsymbol{D} \overset{e-1}{\boldsymbol{F}}_{M_2,r+1}, \tag{46}
$$

$$
\overset{e}{\mathbf{K}}_{2,i} = \overset{e}{\mathbf{R}}_{2,i} - b_{2r} d_{iM_2} \overset{e-1}{\boldsymbol{F}}_{M_2,r+1} - b_{6r} d_{iM_2} \overset{e-1}{\boldsymbol{G}}_{M_2,r+1}, \tag{47}
$$

$$
\overset{e}{\mathbf{K}}_{3,i} = \overset{e}{\mathbf{R}}_{3,i} - c_{2r} d_{iM_2} \overset{e-1}{\boldsymbol{F}}_{M_2,r+1} - c_{7r} d_{iM_2} \overset{e-1}{\boldsymbol{\theta}}_{M_2,r+1}. \tag{48}
$$

Results and Discussion

The natural convection flow from a vertical permeable equations are derived and solved using multi-domain bivariate spectral collocation method. This is done taking into account the normal magnetic field to the surface of the plates. Also, thermal radiation and the Hall current effects are taken into consideration.

	Saha et al. [17]		MBQLM	
ξ	$f''(0,\xi)$	$\theta'(0,\xi)$	$f''(0,\xi)$	$\theta'(0,\xi)$
2	0.706	1.4028	0.7088928	1.4026916
10	–	–	0.1428570	7.0000000
20	0.0714	13.9995	0.0714227	14.0000000
40	0.0357	27.9985	0.0340195	27.9997087
50	0.0285	349981	0.0247535	34.9964783
60	0.0238	41.9977	0.0182251	41.9806430
70	0.0204	48.9974	0.0140161	48.9328200
80	0.0178	55.9971	0.0115996	55.8259543

Table 2: Comparison of Multi-domain solution local skin friction and the Nusselt number against the transpiration parameter ξ while $Pr = 0.7$, $M = 0.5$, $m = 100$ against the Saha et al results [17]

Table 1 shows the comparison results between the current results and the literature results [17]. The table displays the local skin friction and the Nusselt number with respect to the transpiration parameter ξ ranging from 0 to 80 while $Pr = 0.7$, $M = 0.5$, $m = 100$. It is observed that for the increasing value of the transpiration parameter xi the value of the local skin friction coefficient turn to increase near the leading edge, and then diminished slowly. The local Nusselt number coefficient increases rapidly. This observation validates that the solutions of large transpiration number are in agreement with the literature [17].

We also look at the residual error results in order to ensure that our numerical scheme is accurate. The convergence error results are shown in Figures 2, 3 and 4 for velocity, temperature and temperature profiles.

Figures 5 to 7 shows the tangential velocity, transverse velocity and temperature profiles, respectively, for $M = 0.5$, $m = 2$, $R = 1$ and $Pr = 0.01$ for different values of ξ. The tangential

velocity profile, in Figure 5, decreases as the transpiration parameter ξ is increased. This shows that the local maximum values of the velocity profile occurs at the area of the boundary layer. The same observation is shown in Figure 6 on the transverse velocity. Figure 7 shows that the temperature profiles decreases as the transpiration parameter is increased. The momentum and thermal boundary layer thickness decreases with the increasing values of ξ due to suction effects of the surface mass transfer.

Magnetic field parameters effects are presented in Figures 8 and 9. Tangential velocity profiles decrease with increase in magnetic parameter but the transverse velocity increases with an increase in the magnetic field parameter.

The effect of thermal radiation parameter is presented in Figures 10 to 12. The thermal radiation parameter increases both the tangential and transverse velocity profiles. It also increases the temperature profiles of the fluid. This is due to the decrease in values of R leading to a decrease in Rosselenda radiation absorptivity k_1. Also, an increase in temperature has a direct effect on the buoyancy force which in turn iniduces more flow causing the tangential and transverse velocities to increase.

Conclusion

This paper has presented a recently developed multidomain quasilinearisation method for solving general non-linear differential equations. The multidomain quasilinearisation method is developed based on bivariate spectral quasilinearisation method (BSQLM). The main goal of the current study is to apply this method in a natural convection flow from a vertical plate with uniform surface temperature. The method proves to be efficient especially for large transpiration parameter. Velocity, temperature and temperature profiles are also analysed here. From these investigations we can conclude:

- MD-SQLM overcomes the similarity transformation barrier of not capturing solutions at large transpiration parameter values.
- Increase in the transpiration parameter decreases the momentum and thermal boundary layer
- Thermal radiation parameter increases the tangential velocity, transverse velocity and temperature profiles.

References

[1] H. Sato, The Hall Effect in the Viscous Flow of Ionized Gas between Two Parallel Plates under Transverse Magnetic Field. Journal of the Physical Society of Japan, 16,(1961) 1427-1433.

[2] T. Yamanishi, Hall Effect in the Viscous Flow of Ionized Gas through Straight Channels. 17th Annual Meeting, Physical Society of Japan, 5,(1962) 29.

[3] A. Sherman, and G.W. Sutton, Magnetohydrodynamics.Evanston, 173-175.

[4] K.R. Sing, T.G. Cowling, Thermal convection in magnetohydrodynamic boundary layers, J. Mech. Appl. Math. 16(1963) 1–5.

[5] E.M. Sparrow, R.D. Cess, The effect of magnetic field on free convection heat transfer, Int. J. Heat Mass Transfer 3 (1961) 267–274.

[6] A.S. Gupta, Flow of an electrically conducting fluid past a porous flat plate in the presence of a transverse magnetic field, J. Appl. Math. Phys. (ZAMP) 11 (1960) 43–50.

[7] Katagiri, M. The Effect of Hall Currents on the Viscous Flow Magnetohydrodynamic Boundary Layer Flow Past a Semi-Infinite Flat Plate. Journal of the Physical Society of Japan, 27, 1051–1059, 1969.

[8] I. Pop, and T. Watanabe, Hall Effect on Magnetohydrodynamic Free Convection about a Semiinfinite Vertical Flat Plate. International Journal of Engineering Science, 32,(1994) 1903-1911.

[9] M. Wahiduzzaman, R. Biswas, M.D. Eaqub Ali, M.D. S. Khan, Numerical solution of MHD convection and ass transfer flow of viscous incompressible fluid about an inclined plate with Hall current and constant heat flux, Journal of Applied Mathematics and Physics, 3 1688–1709, 2015.

[10] W. G. England and A. F. Emery, Thermal radiation effects on laminar free convection boundary layer of an absorbing gas, Journal of Heat Transfer, vol. 31, pp. 37-44, 1969..

[11] R. S. R. Gorla and I. Pop, Conjugate heat transfer with radiation from a vertical circular pin in a non-newtonian ambient medium, Warme- und Stoffubertragung, vol. 28, no. 1-2, pp. 11-15, 1993.

[12] A. Raptis, Radiation and free convection flow through a porous medium, International Communications in Heat and Mass Transfer, vol. 25, no. 2, pp. 289-295, 1998.

[13] M. Abd El-Aziz, Thermal radiation effects on magnetohydrodynamic mixed convection flow of a micropolar fluid past a continuously moving semi–infinite plate for high temperature differences, Acta Mechanica, vol. 187, no. 1-4, pp. 113-127, 2006.

[14] M. Abd El-Aziz, Thermal–diffusion and diffusion–thermo effects on combined heat and mass transfer by hydromagnetic three-dimensional free convection over a permeable stretching surface with radiation, Physics Letters A, vol. 372, no. 3, pp. 263-272, 2008.

[15] M. Abd El-Aziz, Radiation effect on the flow and heat transfer over an unsteady stretching sheet, International Communications in Heat and Mass Transfer, vol. 36, no. 5, pp. 521-524, 2009.

[16] L. K. Saha, S. Saddiqa, M. A. Hossain. "Effect of Hall current on MHD natural convection flow from vertical permeable flat plate with uniform surface heat flux." Applied Mathematics and Mechanics (English edition) 32. Vol 9(2011): 1127–1146.

[17] L. K. Saha, M. A. Hossain, R.S.R. Gorla. "Effect of Hall current on MHD natural convection flow from vertical permeable flat plate with uniform surface temperature." International Journal of Thermal Sciences 46.(2007): 1790–801.

[18] L. N. Trefethen, Spectral Methods in MATLAB, SIAM (2000).

[19] C. Canuto, M. Y. Hussaini, A. Quarteroni, and T. A. Zang, Spectral Methods in Fluid Dynamics, Springer-Verlag, Berlin (1988).

[20] M.A. Hossain, and S.C. Paul, Free convection from a vertical permeable circular cone with non-uniform surface temperature. Acta Mechanica, 151(1–2) 103–114 (2001) doi:10.1007/BF01272528.

[21] S. S. Motsa, V. M. Magagula, and P. Sibanda, "A Bivariate Chebyshev Spectral Collocation Quasilinearization Method for Nonlinear Evolution Parabolic Equations," The Scientific World Journal, vol. 2014, Article ID 581987, 13 pages, 2014. doi:10.1155/2014/581987

[22] K.A. Yih, MHD forced convection flow adjacent to a non-isothermal wedge, Int. Comm. Heat Mass Transfer, (26) (1999) 819-827

[23] S. Hussain, M.A. Hossain, Natural convection flow from a vertical permeable flat plate with variable surface temperature and species temperature, Engineering Computations, Vol. 17 No. 7, 2000, pp. 789-812.

[24] S. S. Motsa, V. M. Magagula, and P. Sibanda. "A Bivariate Chebyshev Spectral Collocation Quasilinearization Method for Nonlinear Evolution Parabolic Equations." Hindawi Publishing Corporation (2014).

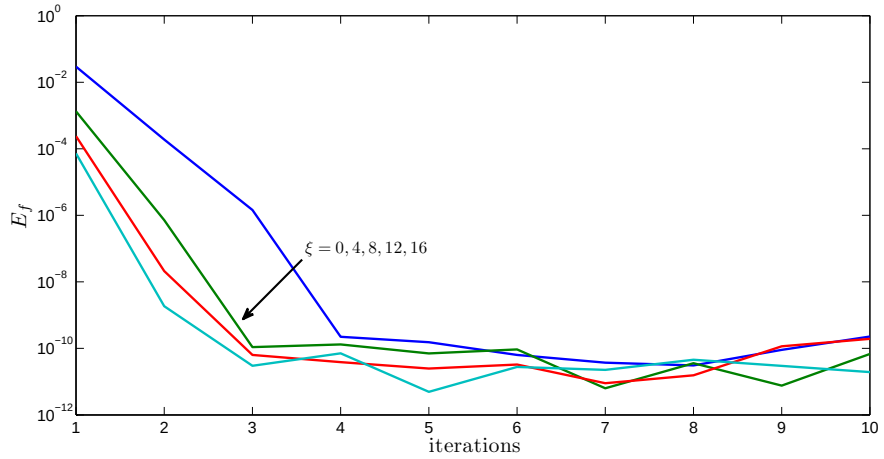

Figure 2: Convergence error in the tangential velocity profile at different values of ξ

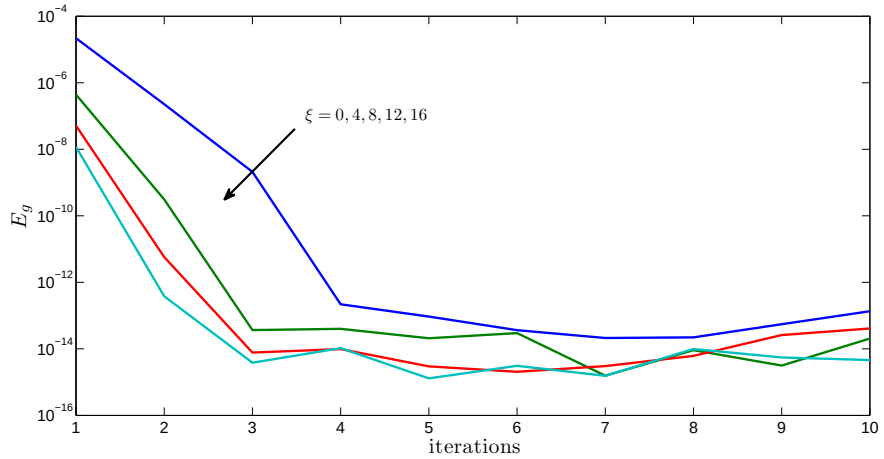

Figure 3: Convergence error in the transverse velocity profile at different values of ξ

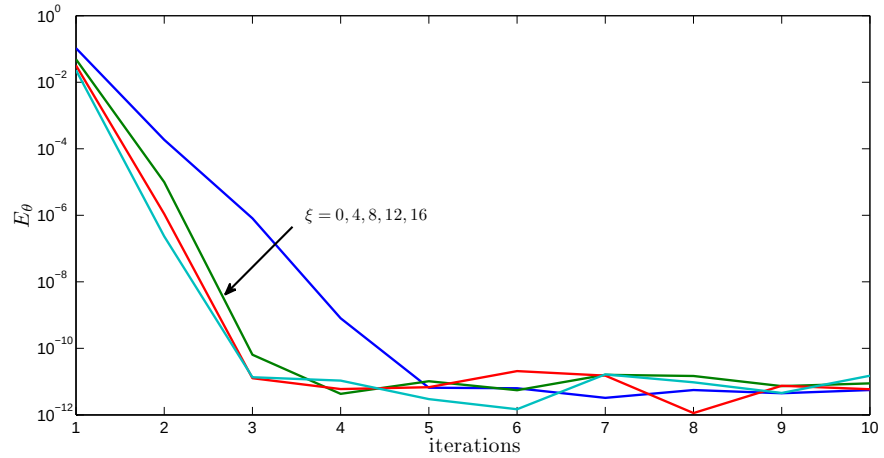

Figure 4: Convergence error in the temperature profile at different values of ξ

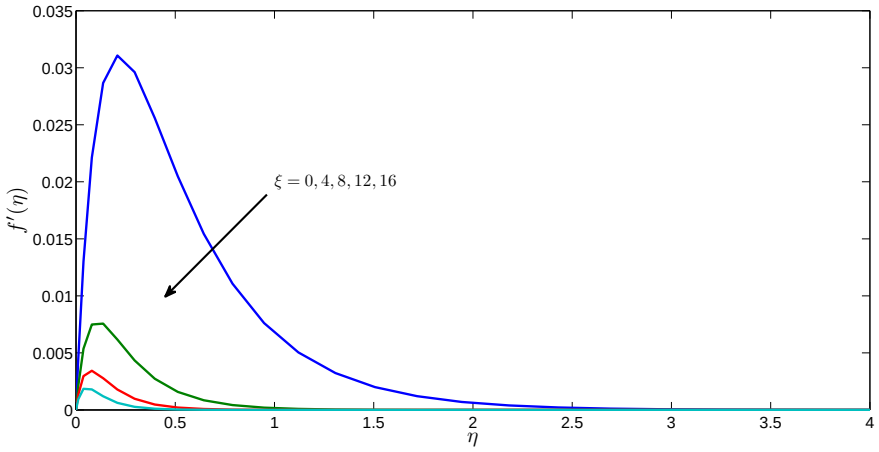

Figure 5: Tangential velocity profile at different values of ξ

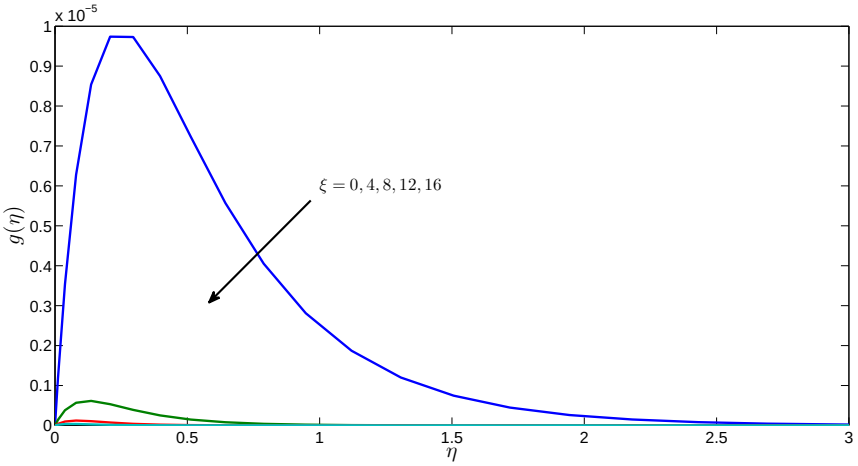

Figure 6: Transverse velocity profile at different values of ξ

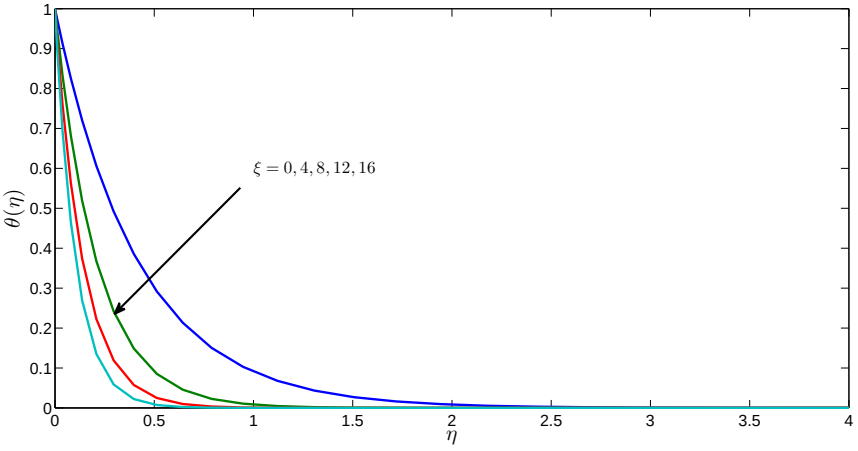

Figure 7: Temperature profile at different values of ξ

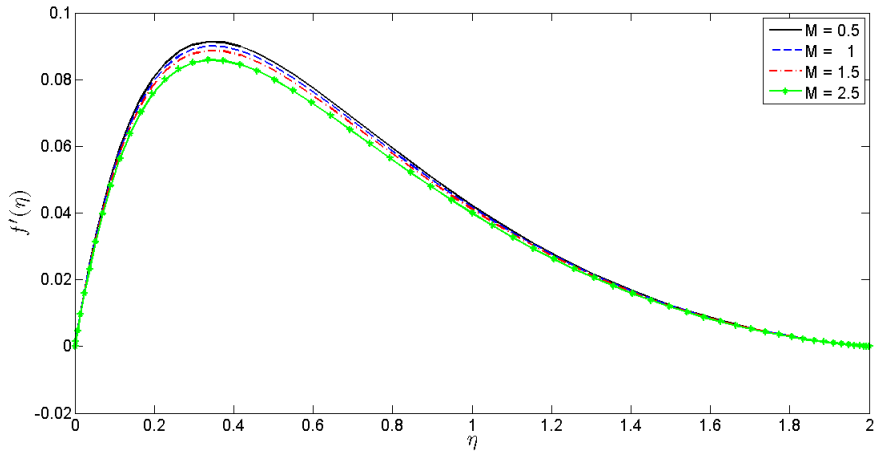

Figure 8: Tangential velocity profile for $R = 3$, $m = 2$, $Pr = 0.7$ at $M = 0.5, 1, 1.5, 2.5$

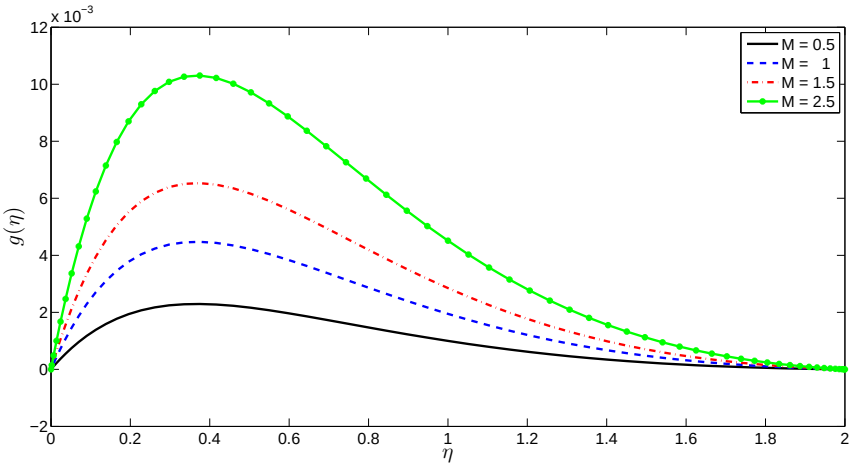

Figure 9: Transverse velocity profile for $R = 3$, $m = 2$, $Pr = 0.7$ at $M = 0.5, 1, 1.5, 2.5$

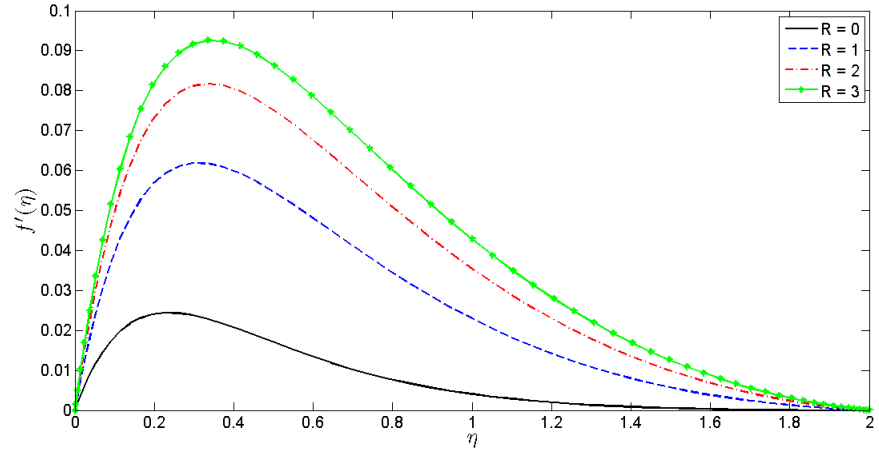

Figure 10: Tangential velocity profile for $M = 1/2$, $m = 100$, $Pr = 0.7$ at $R = 0, 1, 2, 3$

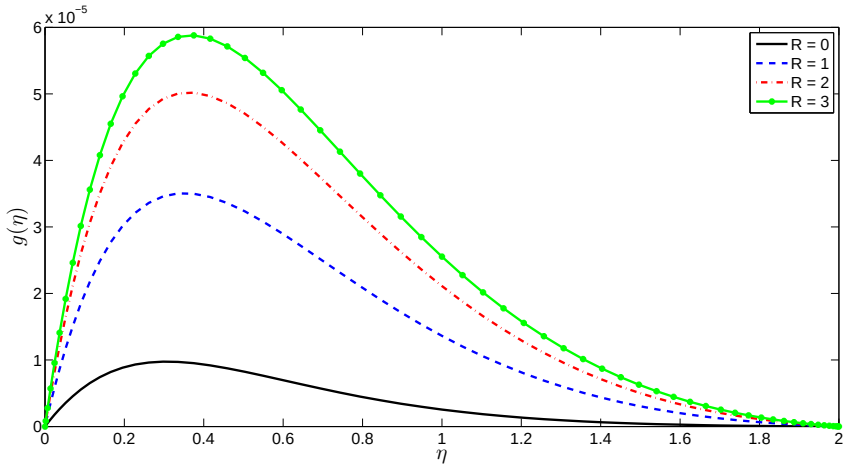

Figure 11: Transverse velocity profile for $M = 1/2$**,** $m = 100$**,** $Pr = 0.7$ **at** $R = 0, 1, 2, 3$

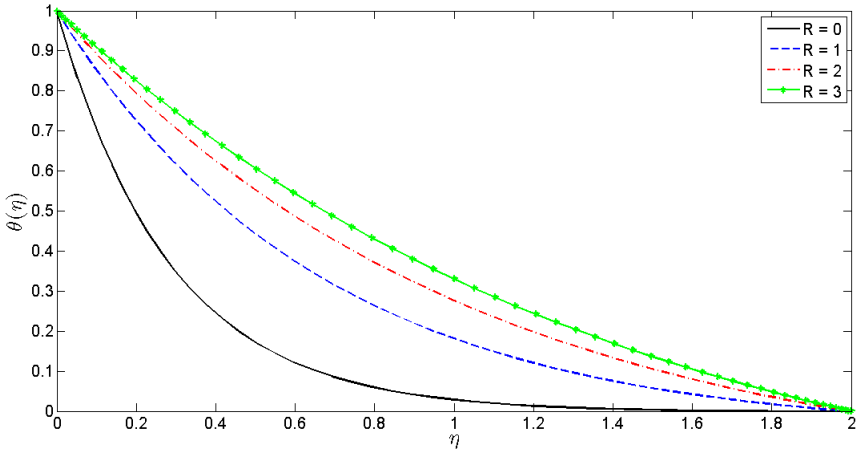

Figure 12: Concentration profile for $R = 3$**,** $m = 2$**,** $Pr = 0.7$ **at** $M = 0.5, 1, 1.5, 2.5$